Current Optics and Photonics
Vol. 4, No. 3, June 2020, pp. 229-237

ISSN: 2508-7266(Print) / ISSN: 2508-7274(Online)
DOI: https://doi.org/10.3807/COPP.2020.4.3.229

Design of a Beam-coupling System for a Chip-integrated Spectrometer with a Discrete Linear Waveguide

Zhiying Liu*, Xin Jiang, and Mingyu Li

Changchun University of Science and Technology, School of Opto-Electronic Engineering, Key Laboratory of Optoelectric Measurement and Optical Information Transmission Technology of Ministry of Education, Changchun 13022, China

(Received December 19, 2019 : revised February 5, 2020 : accepted February 11, 2020)

In this study, a beam-coupling system is designed to improve the coupling efficiency of achip-integrated spectrometer when the waveguide is arranged in a linear and discrete manner. In the proposed system the beam is shaped to be anti-Gaussian, to deposit adequate energy in the edge waveguides. The beam is discretely coupled to the corresponding waveguide by a microlens array, to improve the coupling efficiency, and is compressed by a toroidal lens to match the linear discrete waveguides. Based on the findings of this study, the coupling efficiency of the spectrometer is shown to increase by a factor of 2.57. Accordingly, this study provides a reference basis for the improvement of the coupling efficiency of other similar spectrometers.

Keywords : Chip-integrated spectrometer, Integrated optics, Coupling system, Beam shaping, Microlens array
OCIS codes : (300.6190) Spectrometers; (140.3325) Laser coupling; (140.3510) Lasers, fiber; (220.3620) Lens system design

I. INTRODUCTION

Chip-integrated spectrometers are used extensively in scientific experiments, biomedicine, and in industrial and agricultural production. They realize the transmission of light through an optical waveguide. Optical waveguides typically include one-dimensional waveguides (planar waveguides) and two-dimensional waveguides (such as channel waveguides and ridge waveguides) [1, 2]. Experts have found that when a spectrometer comprises a single-mode ridge waveguide via etching on silicon, it can realize a higher resolution at the same pixel pitch, compared to traditional spectrometers. Such a system is composed of an array of Mach-Zehnder interferometers (MZIs), with the arm-length differences among the MZI array varying linearly. When light is incident upon the waveguide, it is divided by the splitter and enters into the two arms of differing length of the MZI, then interferes by means of the coupler to form an interference pattern. The optical-path difference depends on the difference in arm lengths of the MZI. Compared to traditional spectrometers, the chip-integrated spectrometer contains multiple MZIs and splitters, and the energy of the incident light affects the number of MZIs which can work properly, the free spectral range, and the resolution of the spectrometer [3].

The transmission of the beam depends on the optical fiber, and the coupling efficiency of the fiber determines the transmission rate of the spectral information. Thus, it is important and beneficial to improve the spectral coupling efficiencies of these instruments [4-7].

The chip-integrated spectrometer and optical fiber may be associated with horizontal, grating, or direct couplings. Horizontal coupling expands the mode field of the single-mode waveguide by a spot-size converter, and changes the fiber endface to form a lens fiber for coupling [8]. Grating coupling uses a grating coupler to join the fiber and the spectrometer, but requires matching of the transverse width of the grating to the core size of the fiber [9]. Direct

*Corresponding author: lzyccccc@126.com, ORCID 0000-0002-0726-8857
Color versions of one or more of the figures in this paper are available online.

coupling is achieved by aligning the endface of the optical fiber with the single-mode waveguide, but the fiber needs to be in contact with the waveguide. At this point, mismatch between the fiber and single-mode waveguide leads to energy losses, as shown in Fig. 1. Coupling of the beams cannot be achieved, based on the aforementioned methods, when numerous single-mode waveguides receive light simultaneously [10, 11].

The traditional coupling method involves transmission of a Gaussian beam, such that the energy is concentrated in its central part. The chip-integrated spectrometer waveguide is a $1 \times n$ linear discrete array. The response of the waveguide array decreases from the center to the edge. Traditional coupling methods cannot match the cross-sectional size, and the beam cannot be distributed on each waveguide discretely, thus causing the loss of light energy at the waveguide gap. Traditional coupling cannot compress the beam in the y direction, but only in the x direction. In summary, the waveguide array of achip-integrated spectrometer will not work properly, owing to the insufficient light energy, which will affect the free spectral range and resolution of the spectrometer.

In this study, a beam-coupling system is designed for a chip-integrated spectrometer with a discrete linear waveguide. The system couples the beam to each waveguide, thus improving the energy and coupling efficiencies.

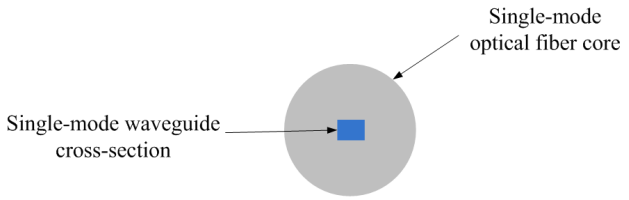

FIG. 1. Comparison of the crosssections of a single-mode fiber and single-mode waveguide.

II. WORKING PRINCIPLE OF THE BEAM-COUPLING SYSTEM INTENDED FOR USE IN ACHIP-INTEGRATED SPECTROMETER WITH A DISCRETE LINEAR WAVEGUIDE

A beam-coupling system for an on-chip spectrometer with a discrete linear waveguide consists of beam shaping, beam spreading, and discrete-beam and linear-matching subsystems, as shown in Fig. 2. First, the Gaussian beam is reshaped by a beam-shaping subsystem, to improve the utilization rate of the edge energy. Second, the beam diameter is expanded by the beam-spreading subsystem, to match the size of the waveguide. Beam separation is then realized by the discrete-beam subsystem, which utilizes energy

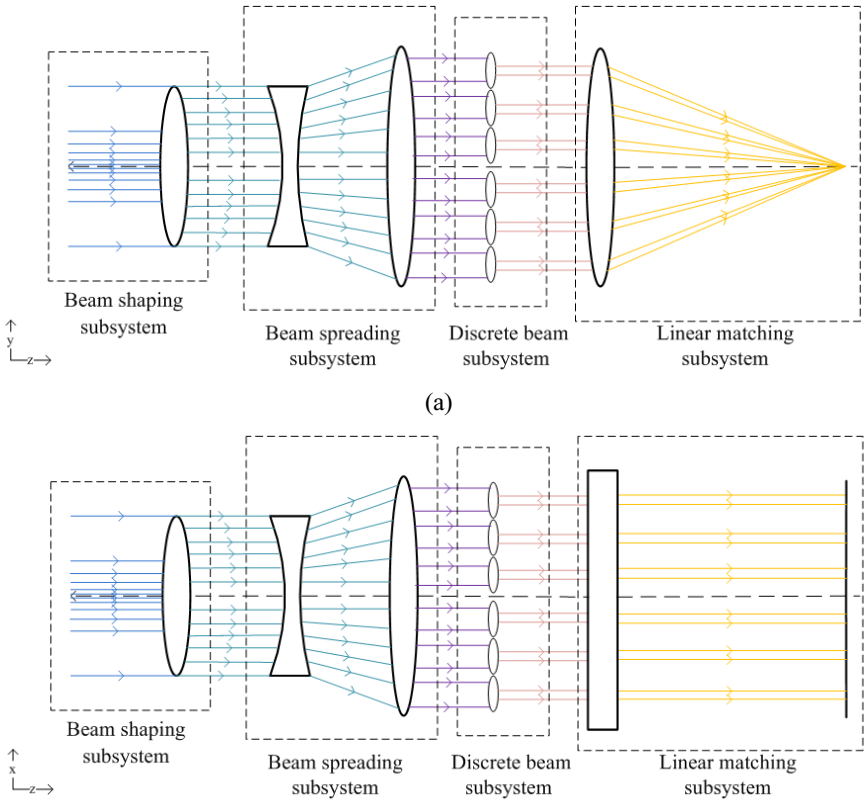

FIG. 2. Schematic diagram of the spectrometer's beam-coupling system: (a) y-z plane, (b) x-z plane.

at the waveguide gap. Finally, the beam is compressed in the *y* direction by a linear-matching subsystem, to match the waveguide array. These four subsystems work together to improve the coupling efficiency of the chip-integrated spectrometer with a discrete linear waveguide.

Figure 2 shows the transmission of the beam in the *y*-*z* and *x*-*z* planes. The fiber is fixed at the left-hand-side end, and the input is a Gaussian beam. The beam exiting from the fiber can be efficiently coupled by the system to the waveguide array placed at the image plane.

2.1. Principle of the Beam-shaping Subsystem

A Gaussian beam is input to the system. The energy distribution of the Gaussian beam, as shown in Fig. 3, is focused in its central part, and only a small fraction of the energy is associated with the edges. A Gaussian beam is not beneficial for coupling efficiency. The Gaussian distribution is expressed by Eq. (1)

$$\mathrm{I}_{in} = A^2(r_1) = A_0^2 \exp^2\left(-\frac{r_1^2}{\omega^2}\right) = I_0 \exp^2\left(-\frac{r_1^2}{\omega^2}\right), \tag{1}$$

where I_0 is the light intensity at the center, A_0 is the amplitude at the center, ω is a parameter related to the beam's cross-sectional radius, and r_1 is the half-diameter of the input beam.

Most existing studies have shaped Gaussian beams into flat-topped beams. However, compared to a flat-topped beam, an anti-Gaussian beam, with low central energy and a significant energy distribution at the edges, offers higher edge energy after longitudinal compression by the linear-matching subsystem. Therefore, the beam-shaping subsystem reshapes the Gaussian distribution into an anti-Gaussian distribution, as shown in Fig. 4.

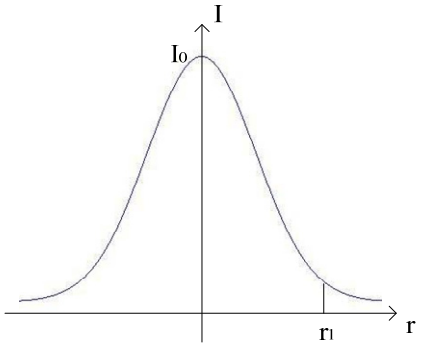

FIG. 3. Energy distribution of a Gaussian beam.

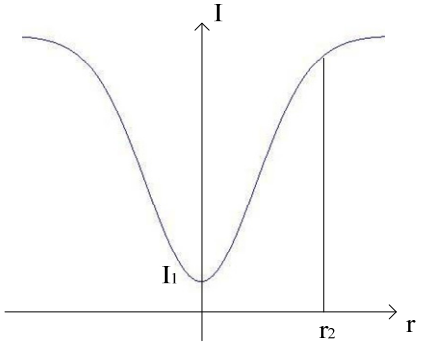

FIG. 4. Energy distribution of an anti-Gaussian beam.

The equation of the intensity distribution of the anti-Gaussian beam can be deduced based on Eq. (2)

$$\mathrm{I}_{out} = -I_0 \exp^2\left(-\frac{r_2^2}{\omega^2}\right) + (I_0 + I_1), \tag{2}$$

where I_1 is the light intensity at the center of the anti-Gaussian beam, and r_2 is the half-diameter of the output beam for the case in which the beam diameter is unchanged, that is, when

$$r_1 = r_2 = r_0, \tag{3}$$

where r_0 is a constant. According to the energy conservation of Eq. (4)

$$\int_0^{r_0} \mathrm{I}_{in} dr_1 = \int_0^{r_0} \mathrm{I}_{out} dr_2, \tag{4}$$

substitution of Eqs. (1) and (2) into (4) leads to

$$I_1 = \frac{2\int_0^{r_0} I_0 \exp^2\left(-\frac{r_1^2}{\omega^2}\right) dr_1 - I_0 r_0}{r_0}. \tag{5}$$

Substitution of Eq. (5) into (2) allows us to deduce the intensity distribution equation of the anti-Gaussian beam. Accordingly, η is set as the proportion of the circular area of energy, and $r'$the radius. Therefore, η can be defined according to Eq. (6)

$$\eta = \frac{\int_0^{r'} \mathrm{I}_{out} dr_2}{\int_0^{r_0} \mathrm{I}_{out} dr_2}. \tag{6}$$

By substituting different values in the range of 0-1, the r' value can be calculated, and the beam-shaping subsystem can be optimized with the use of the function GENC in the ZEMAX software [12-15].

2.2. Working Principle of the Beam-spreading Subsystem

When the incident beam's diameter does not match the width of the optical-waveguide array of the spectrometer, it is necessary to design a beam-spreading subsystem. Based on a telescopic system structure, this subsystem needs to shorten the total length. Thus, the subsystem adopts the inverted Galileo structure, as shown in Fig. 5.

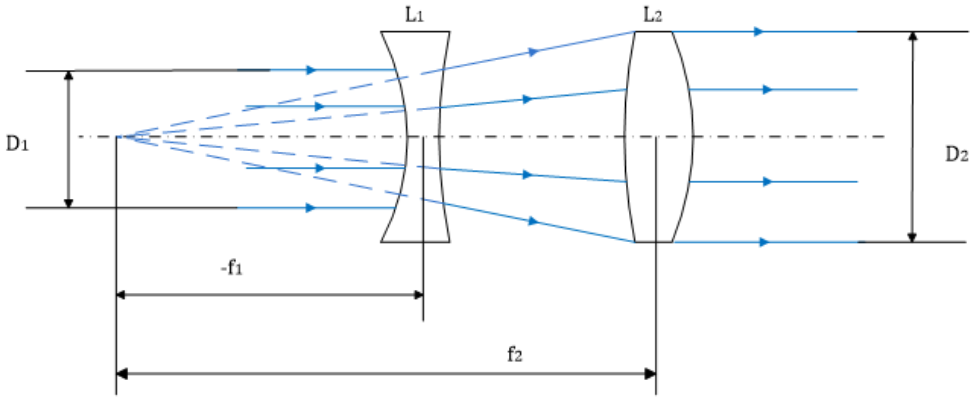

FIG. 5. Diagram of an inverted Galileo structure. D_1 is the diameter of the incident light beam, D_2 is the diameter of the outgoing light, f_1 is the focal length of the first lens, and f_2 is the focal length of the second lens.

2.3. Working Principle of the Discrete-beam Subsystem

2.3.1. Coupling efficiency of a traditional system and the discrete-beam subsystem

The single-mode ridge waveguide of the spectrometer is formed by etching on the silicon-on-insulator (SOI) platform. However, to show the matching between the waveguide array and the discrete-beam subsystem, a single module is used to represent a single-mode ridge waveguide, as shown in Fig. 6. The optical-waveguide structure of the chip-integrated spectrometer is a linearly distributed array with a specific spacing between each waveguide. If the light is compressed directly through the toroidal lens, the light energy at the waveguide gap still will be wasted. When the waveguide's spacing is wide, only a fraction of the light can be utilized, causing a significant reduction in coupling efficiency.

If the number of waveguides is n, the cross-sectional size of the waveguide is $a \times b$, and the spacing of the waveguides is c, the maximum coupling efficiency δ_1 of the traditional method adheres to Eq. (7)

$$\delta_1 = \frac{na}{na + (n-1)c}. \tag{7}$$

If the waveguide gap c is greater than the waveguide length a, then the coupling efficiency of the traditional method $\delta_1 \approx 0$.

In this study, the discrete-beam subsystem can reduce the $(n\text{-}1)c$ term by concentrating energy on the waveguide at its gap. Thus the maximum coupling efficiency δ_2 adheres to Eq. (8)

$$\delta_2 = \frac{na}{na} = 1. \tag{8}$$

Therefore, if the energy losses in the transmission process are neglected, the entire beam energy of the optical fiber will be used in the waveguide.

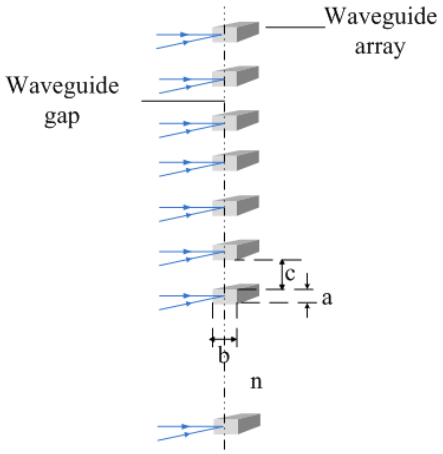

FIG. 6. Matching relationship between the waveguide array and the discrete-beam subsystem.

2.3.2. Design principle of the discrete-beam subsystem

To concentrate the energy on the waveguide, the discrete-beam subsystem needs to converge the light to n waveguides independently. However, this cannot be realized by a traditional optical lens. The discrete-beam subsystem uses a microlens array to match the distribution of the waveguide, thus allowing the independent convergence of rays for each waveguide.

The circular beam is divided into n smaller parts in the x and y directions with a designed $n \times n$ microlens array. The diameter of the microlens element is $a + c$, the sum of the waveguide length and waveguide spacing. The circular beam is divided into a small $n \times n$ beam array by the microlens array, and each small beam diameter is equal to a, which is the same as the waveguide length. Therefore the discrete-beam subsystem can improve the coupling efficiency based on the convergence of the light.

The microlens array structure is shown in Fig. 7. A ray is converged independently by each microlens in the first array, and is diverged independently in the second microlens array, to ensure that light is emitted in parallel directions [16].

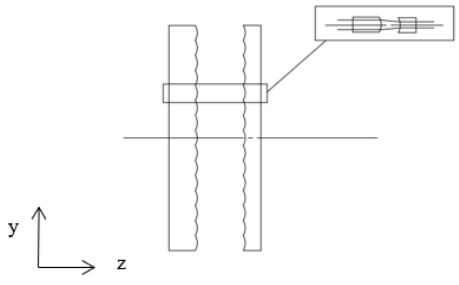

(a)

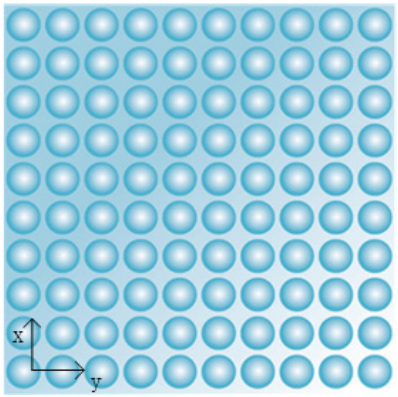

(b)

FIG. 7. Diagram of the microlens array.

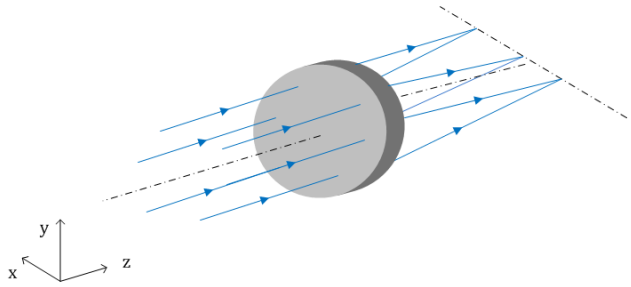

FIG. 8. Diagram of the linear-matching subsystem.

2.4. Working Principle of the Linear-matching Subsystem

The optical-waveguide structure of the chip-integrated spectrometer is linearly distributed in a $1 \times n$ arrangement, while the small beam array has a circular distribution, as shown in Fig. 8. The toroidal lens is designed to compress the rays in the y direction and maintain the original direction of propagation in the x direction. Therefore the spots are distributed linearly on the image plane, to meet the system requirements.

III. DESIGN OF THE BEAM-COUPLING SYSTEM FOR ACHIP-INTEGRATED SPECTROMETER WITH A DISCRETE LINEAR WAVEGUIDE

3.1. System Design Parameters

The design parameters of this system are listed in Table 1.

TABLE 1. System design parameters

System parameters	Value
Spectral range	0.38~0.78 μm
Incident light diameter	1.8 mm
Angle of divergence of incident light	<1 mrad
Number of waveguides $n \times 1$	201 × 1
Waveguide crosssection $a \times b$	3 μm × 1.5 μm
Waveguide gap c	20 μm
Numerical aperture of waveguide	0.12

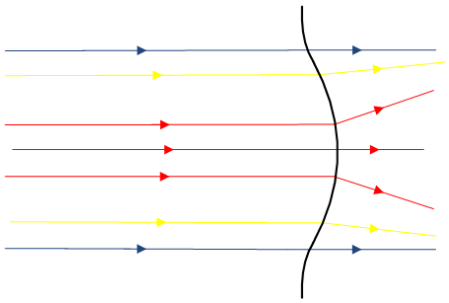

FIG. 9. Schematic diagram of light refraction.

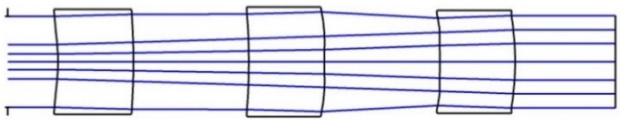

FIG. 10. Structure of the beam-shaping subsystem.

3.2. Design of the Beam-shaping Subsystem

As shown in Fig. 9, the refraction directions of rays at each position are different when the Gaussian beam is refracted through the lens. The central rays should be diverged, and the edge rays should be kept along the original direction of propagation. Therefore, the radius of lens curvature is different at each position. The farther away one is from the optical axis, the greater the radius of the curvature is. Thus, the lens surface adheres to the mathematical formulation of an aspheric surface, as expressed by Eq. (9)

$$z = \frac{cr^2}{1+\sqrt{1-(1+k)cr^2}} + \alpha_1\gamma^2 + \alpha_2\gamma^4 + \alpha_3\gamma^6 + \alpha_4\gamma^8 + \alpha_5\gamma^{10} + \alpha_6\gamma^{12} + \alpha_7\gamma^{14} + \alpha_8\gamma^{16}. \quad (9)$$

Figure 10 is the structure of the beam-shaping subsystem. Referring to the Galileo structure, it should consist of a concave and a convex aspheric lens. However, the asphericity of the two lenses is exaggerated. Considering the processing of the aspheric lens, the concave lens can be divided into two other lenses.

As shown in Fig. 11, the spots in the central region are sparse, while the edge spots are dense. Figure 12 is the energy distribution of the beam-shaping subsystem. As can be observed, the central region takes up less energy, while the edges take up more. Based on Figs. 11 and 12, the emitted light from the beam-shaping subsystem has an anti-Gaussian distribution, and thus achieves the subsystem's requirements.

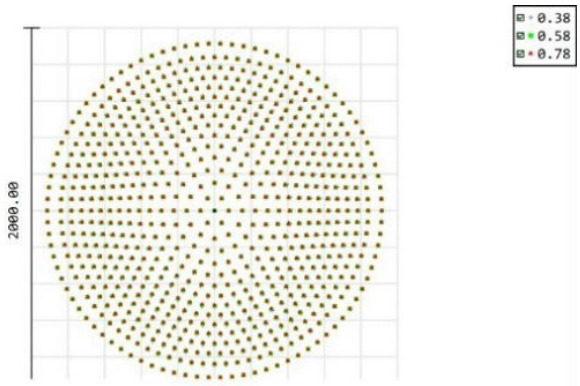

FIG. 11. Spot diagram of the beam-shaping subsystem.

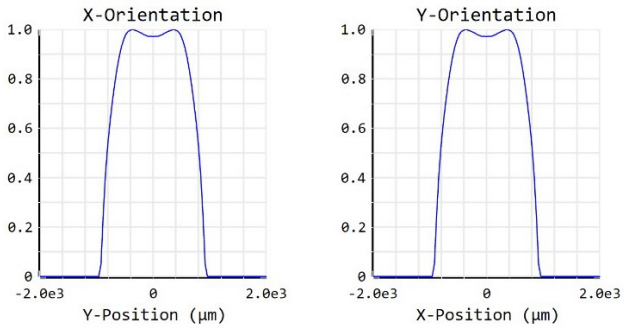

FIG. 12. Energy distribution of the beam-shaping subsystem.

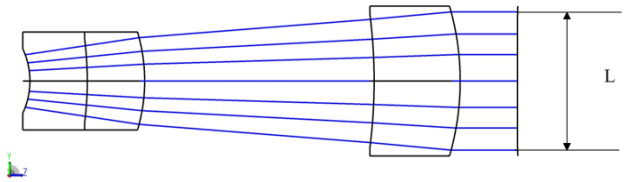

FIG. 13. Structure of the beam-spreading subsystem.

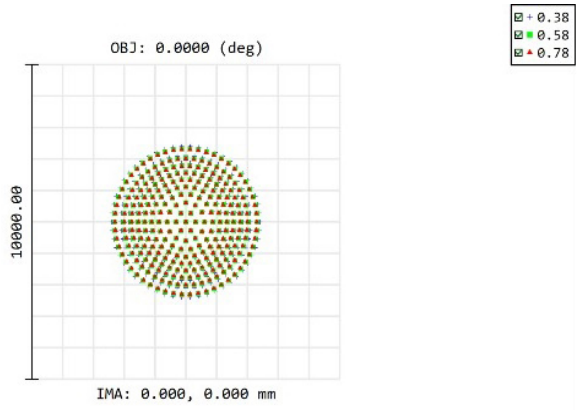

FIG. 14. Spot diagram of the beam-spreading subsystem.

3.3. Design of the Beam-spreading Subsystem

As shown in Fig. 13, the beam-spreading subsystem references the inverted Galileo structure. Because the diameter of a microlens-array element in the discrete beam subsystem is $(a + c)$, the diameter of the emitted beam from the beam-spreading subsystem L *o*beys Eq. (10)

$$L = n(a + c), \tag{10}$$

where n is the number of waveguides, a is the length of a waveguide, and c is the spacing of the waveguides. Substituting the parameters listed in Table 1 into Eq. (10) can yield the value of the diameter L, which is equal to 4.623 mm. The spectral range of the system is broad, and chromatic aberration should be considered; therefore, the concave lens is replaced by a doublet lens, as shown in Fig. 13, and the central spots are sparse while the edge spots are dense, as shown in Fig. 14.

3.4. Design of the Discrete-beam Subsystem

Figure 15 is the structure of the microlens-array element that converts the beam's diameter (23 μm)—the sum of the waveguide length and spacing—to the waveguide length (3 μm). It can be clearly seen in Fig. 16 that the light spot distribution is uniform. A 201 × 201 microlens array was defined with the "User Defined" command in ZEMAX. Eventually, the beam was divided into 201 × 201 smaller beams to achieve the subsystem's requirements.

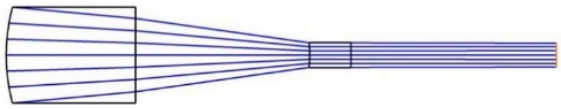

FIG. 15. Element structure of the microlens array.

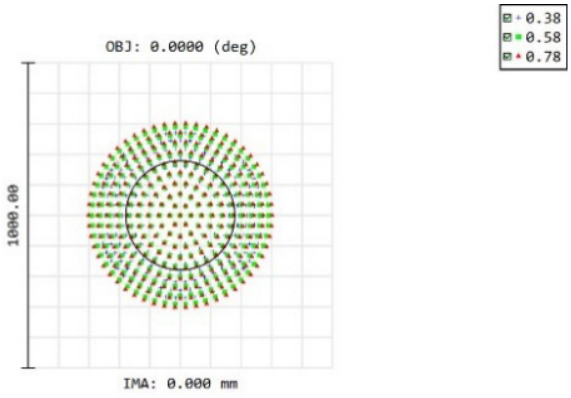

FIG. 16. Spot diagram of a microlens element.

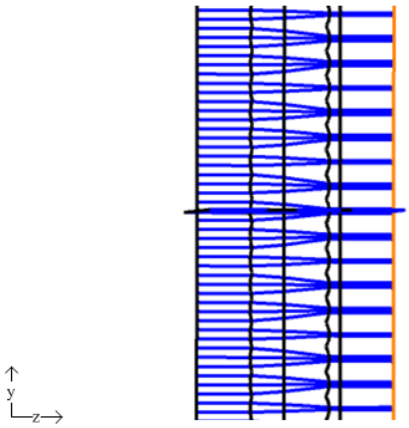

FIG. 17. Partial enlargement of the microlens array.

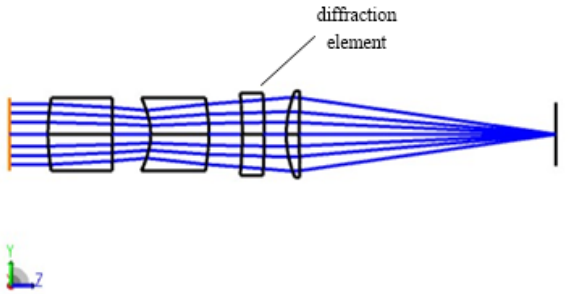

(a)

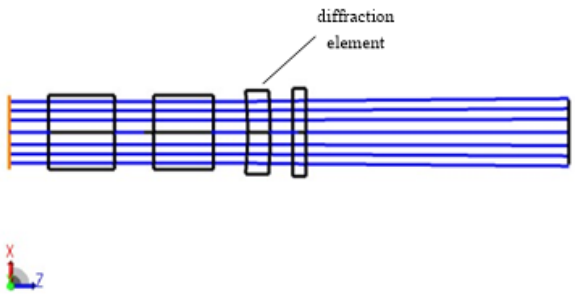

(b)

FIG. 18. Structure of the linear-matching subsystem: (a) *y-z* plane, (b) *x-z* plane.

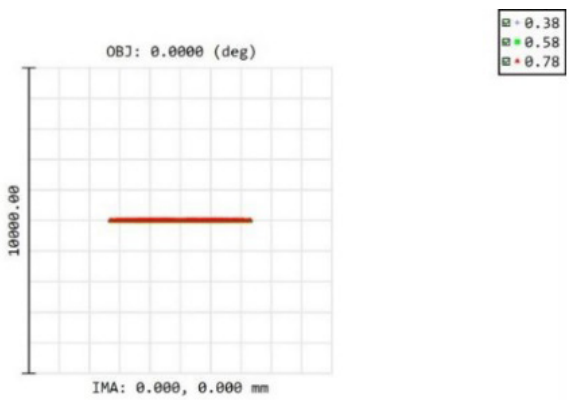

FIG. 19. Spot diagram of the linear-matching subsystem.

A partial enlargement of the microlens array is shown in Fig. 17. The beam is divided into individual, smaller beams to achieve the subsystem's requirements. Given that the first microlens array concentrates the smaller beams, there is no light at the lens unit's connection.

Substitution of the parameters listed in Table 1 into Eq. (7) yields the value of the maximum coupling efficiency of the traditional coupling method δ_1, which equals just 0.137.In this study the system divides the spots, couples the light at the gap to the waveguide structure, and eliminates the $(n\text{-}1)c$ term. The theoretical value of the coupling efficiency δ_2 is 1.

3.5. Design of the Linear-matching Subsystem

As shown in Fig. 18, the ray is compressed in the *y* direction by toroidal lenses. The spectral range of the system is broad, so chromatic aberration should be considered. The diffraction element is set to reduce the chromatic aberration. In this case, the numerical aperture of the linear matching subsystem is 0.074, which is less than the numerical aperture of the waveguide in Table 1. As shown in Fig. 19, the beam is compressed into a linear distribution.

IV. OUTCOMES OF THE OPTICAL-SYSTEM DESIGN

Splicing the four subsystems described in Section 3 yields the results shown in Fig. 20. Effectively, this is the structure of the system in the *y-z* and *x-z* planes. The system needs no contact between the optical fiber and the chip-integrated spectrometer. As shown in Fig. 21, the spots are distributed discretely to match the waveguide array, and the waveguides at the edgesreceive adequate energy. As shown in Fig. 22, the energy is concentrated on the waveguide array. The system proposed herein can improve the beam's accuracy and coupling efficiency.

Because the incident light of the microlens array is not perfectly parallel in the actual optical design. After the light passes through the micro lens array and the toroidal lens, each discrete spot formed is different. And the actual spots are larger than the waveguide, the energy cannot be fully utilized. The actual coupling efficiency can be calculated based on the sampling spots according to Eq. (11)

$$\delta_3 = \frac{ab}{pq}, \tag{11}$$

where a and b respectively denote the length and width of the waveguide, p and q respectively denote the length and width of the actual sampling spot, and δ_3 is the actual coupling efficiency. Discrete spots were selected, as indicated in Table 2.

According to Table 2, the average actual coupling efficiency of the system is 0.352, which is 2.57 times as

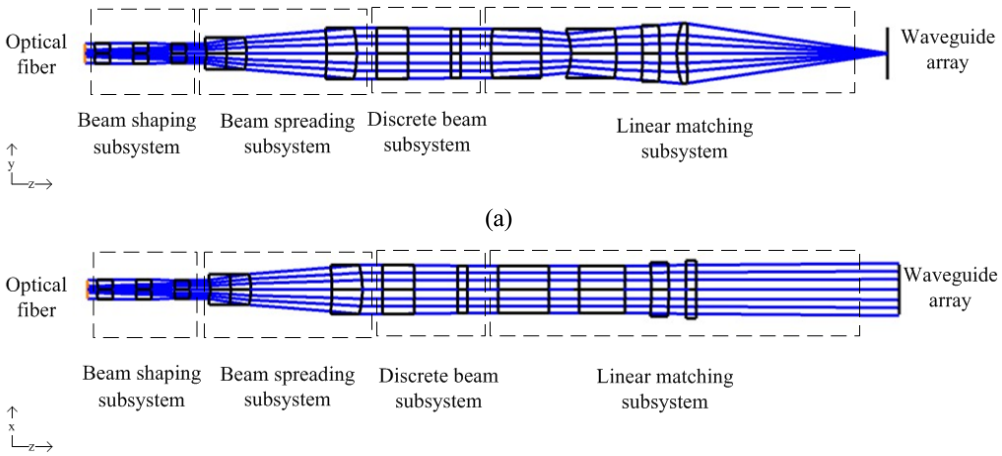

FIG. 20. Structure of the beam-coupling system for achip-integrated spectrometer with a discrete linear waveguide, along the (a) *y*-*z* and (b) *x*-*z* planes.

FIG. 21. Spot diagram of the beam-coupling system for a chip-integrated spectrometer with a discrete linear waveguide.

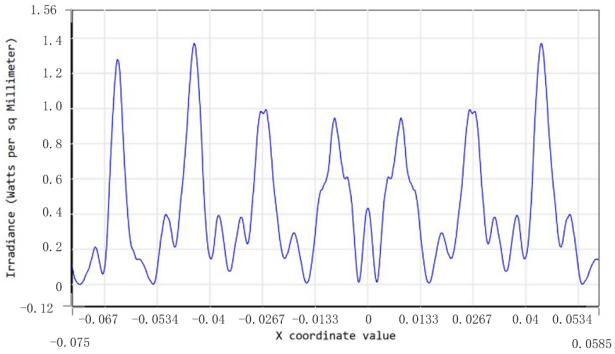

FIG. 22. Energy distribution of the beam-coupling system for a chip-integrated spectrometer with a discrete linear waveguide.

TABLE 2. Spot sampling data

Spot length p (μm)	Spot width q (μm)	Actual coupling efficiency δ_3
0.96	4.80	0.312
4.3	4.60	0.228
6.0	2.794	0.268
4.1	2.544	0.431
5.0	1.723	0.522

large as the *ideal* coupling efficiency of the traditional method. If the average transmittance of the lenses were 0.99, then the average actual coupling efficiency would be 0.315, which is 2.30 times as large as the ideal efficiency of the traditional method.

The maximum actual coupling efficiency is 0.522, which is 3.81 times as large as the ideal efficiency of the traditional method, while the minimum actual coupling efficiency is 0.228, which is still higher than the ideal coupling efficiency of the traditional method (0.137). Therefore, it is feasible to improve beam-coupling efficiency based on the use of the beam-coupling system proposed in this study.

V. SUMMARY

In this study, we design a beam-coupling system for a chip-integrated spectrometer with a discrete linear waveguide to ensure that the waveguide can receive sufficient response energy at the edges. Furthermore, the system matches light with the 201 × 1 linear waveguide array of the spectrometer. It does not need contact between the optical fiber and the chip-integrated spectrometer, which avoids wear. The system can improve the coupling efficiency by a factor of 2.57. Its structure is simple, it is easy to set up, and it does not require manual adjustments. It solves the problem of beam coupling in the case of the discrete linear waveguide of a chip-integrated spectrometer, provides a reference for beam coupling for that type of spectrometer, and is practically useful.

ACKNOWLEDGMENT

This work is funded by National Natural Science Foundation of China (NSFC), grant no.61805025. The authors thank the scholars at the Optical Testing and Analysis Center (OTAC) for their support and assistance in this work.

REFERENCES

1. C.-X. Liu, S. Cheng, J.-H. Zhao, W.-N. Li, W. Wei, B. Peng, and H-.T. Guo, "Monomode optical planar and channel waveguides in Yb^{3+}-doped silicate glasses formed by helium ion implantation," Opt. Laser Technol. **44**, 10-14 (2013).
2. Y. Wang, X.-L. Shen, Q.-F. Zhu, and C.-X. Liu, "Optical planar and ridge waveguides in terbium gallium garnet crystals produced by ion implantation and precise diamond blade dicing," Opt. Mater. Express **8**, 3288-3294 (2018).
3. M. Yang, M. Li, and J.-J. He, "Static FT imaging spectrometer based on a modified waveguide MZI array," Opt. Lett. **42**, 2675-2678 (2017).
4. M.-C. Oh, W.-S. Chu, K.-J. Kim, and J.-W. Kim, "Polymer waveguide integrated-optic current transducers," Opt. Express **19**, 9392-9400 (2011).
5. K. S. Chiang, "Development of optical polymer waveguide devices," Proc. SPIE **7605**, 760507 (2010).
6. G. Chen, Z.-Y. Wen, Z.-Q. Wen, Z.-P. Jiang, and S.-L. Huang, "The experimental test of a reflecting hybrid micro fiber spectrometer," Spectrosc. Spectral Anal. **23.6**, 1232-1236 (2003).
7. J. Ozhikandathil and M. Packirisamy, "Nano-islands integrated evanescence-based lab-on-a-chip on silica-on-silicon and polydimethylsiloxane hybrid platform for detection of recombinant growth hormone," Biomicrofluidics **6**, 046501 (2012).
8. T. Shoji, T. Tsuchizawa, T. Watanabe, K. Yamada, and H. Morita, "Low loss mode size converter from 0.3 μm square Si wire waveguides to singlemode fibres," Electron. Lett. **38**, 1669-1670 (2002).
9. F. V. Laere, G. Roelkens, M. Ayre, J. Schrauwen, D. Taillaert, D. V. Thourhout, T. F. Krauss, and R. Baets, "Compact and highly efficient grating couplers between optical fiber and nanophotonic waveguides," J. Lightwave Technol. **25**, 151-156 (2007).
10. B. Zhang and Z.-Y. Wen, "Development and performance test of a micro fiber spectrometer," Semicond. Optoelectron. **28**, 147 (2007).
11. D. Benedikovic, P. Cheben, J. H. Schmid, D.-X. Xu, B. Lamontagne, S. Wang, J. Lapointe, R. Halir, A.-O. Moñux, S. Janz, and M. Dado, "Subwavelength index engineered surface grating coupler with sub-decibel efficiency for 220-nm silicon-on-insulator waveguides," Opt. Express **23**, 22628-22635 (2015).
12. K. Feng and J. Li, "Design of aspherics lenses shaping system on Gaussian beam," Opto-Electron. Eng. **40**, 127-132 (2013).
13. J. A. Hoffnagle and C. M. Jefferson," Beam shaping with a plano-aspheric lens pair," Opt. Eng. **42**, 3090-3100 (2003).
14. C. Wang and D. L. Shealy, "Design of gradient-index lens systems for laser beam reshaping," Appl. Opt. **32**, 4763-4769 (1993).
15. S. Kim, D. A. Westly, B. J. Roxworthy, Q. Li, A. Yulaev, K. Srinivasan, and V. A. Aksyuk, "Photonic waveguide to free-space Gaussian beam extreme mode converter," Light: Sci. Appl. **7**, 72 (2018).
16. W. Choi, R. Shin, J. Lim, and S. Kang, "Design methodology for a confocal imaging system using an objective microlens array with an increased working distance," Sci. Rep. **6**, 33278 (2016).